Detection and localization of defects in cable sheath of cross-bonding configuration by sheath currents

Marina A. Shokry, Abderrahim Khamlichi, Fernando Garnacho, Julio Martinez, Fernando Álvarez

***Abstract*—Nowadays many researchers are focusing on on-line condition monitoring of high-voltage (HV) insulated cable systems to prevent failures. With the aim of reducing the voltage induced in the cable sheaths, cross-bonding (CB) grounding cable systems are used in long distance power transmission lines. This paper proposes a new criterion for the detection and localization of defects that might occur in the cables sheath when a CB configuration is adopted. The criterion proposed can be applied at different levels of load current. For the application of the criterion the cable system under evaluation is modeled using the ATP software. Various practical cases were studied showing the effectiveness of the criterion for the detection and localization of different types of defects in simulated cable systems. Furthermore, in order to validate the criteria adopted for the defect detection, based on the ATP model, a real defected case was evaluated. The results obtained proved that this criterion is suitable for the detection and localization of defects in the cables sheath, when on-line measurements are performed in monitoring applications.**

***Index Terms*— condition monitoring, current measurements, electric breakdown, cable shielding, sheath current, fault current.**

I. Introduction

HV insulated power cables form an essential part in the distribution and transmission network grids in the urban areas due to their high reliability, environmental friendliness and visual impact. Although the life time of insulated power cables may exceed 30 years, if proper start-up and maintenance policies are not carried out, this period can be considerably reduced. Thus, on-line diagnostic techniques are becoming commonly applied on HV and MV power grids.

For utilities, the main advantage of performing on-line measurements for the assessment of the cable sheath condition is that the interruption of the power supply is not required, while in off-line measurements a planned shutdown is needed [1-4].

This work has received funding from the European Union's Horizon 2020 research and innovation programme under the Marie Sklodowska-Curie grant agreement No 676042. The authors also appreciatively acknowledge the Spanish TSO for providing the field data which helped in the development of this paper.

M. A. Shokry is with the Universidad de politécnica de Madrid, Spain (madel@lcoe.etsii.upm.es)

A. Kamlichi is with the Universidad de politécnica de Madrid, Spain, (ak@lcoe.etsii.upm.es)

F.Garnacho is with the fundación para el fomento de la innovación industrial, LCOE, Madrid, Spain, (fgarnacho@lcoe.etsii.upm.es)

J. Martinez is with the Universidad de politécnica de Madrid, Spain (julio.martinezm@upm.es)

F. Alvarez is with the Universidad de politécnica de Madrid, Spain (fernando.alvarez@upm.es)

When a cable length exceeds 1 km, Cross bonding (CB) configuration or a combination between CB and Single point (SP) are adopted to reduce the induced current in the cable sheaths in order to avoid excessive losses [5-7].

The sheath currents depend on the asymmetry of the load currents, the laying methods, the length of the minor sections and the external electromagnetic field [6].

A good number of cable defects cause excessive sheath current [5].The feasibility of detecting a fault in the cable over-sheath by monitoring the sheath currents to ground at the end of the cross-bonded sections is presented in [4].

Different criteria (depending on the type of the defect) were developed by Xiang Dong *et al.* [1] to detect defects in cable sheaths by measuring sheath currents when CB configurations without transposition in flat formation are adopted. Although this study is very efficient to detect the defects in cable sheath, the influence of the load current and the unbalance of the lengths of the minor sections have not studied on the criteria proposed. Moreover, the feasibility of detecting sheath defects by measuring sheath currents on the CB configuration with cable transposition have not studied before.

This paper presents a generic novel criterion for detecting and localizing defects in the cable sheaths: open circuit in sheath loop, breakdown between sectionalized sheaths, inadequate sheath connection in linkbox and flooding in linkbox, for CB with and without transposition, for any percentage of load currents. Simple codes from #0 to #4 are introduced to represent the degree of change of the sheath current in case of a defect. Furthermore, in this criterion the influence of the cable formation type (in trefoil or flat) and the unbalance in CB minor sections are considered. In addition, the criterion has been improved by subtracting the capacitive component of the sheath current to validate the proposed criterion under low levels of load current.

II. Problem Statement

A. Theoretical equations

A CB configuration is formed by 3 minor sections. Ideally the three sections should have the same length (balanced CB), however, in practice, they may slightly differ in length (L_1, L_2, and L_3); nevertheless, the difference in lengths should not be higher than 30% in any case. In each minor section, three single phase cables of equal lengths are lied in. There are two types of configuration for cable laying: trefoil formation and flat formation, as shown in Fig. 1.

The CB configuration without cable transposition is used for trefoil formation (Fig.2a), whereas CB with cable transposition is usually applied on flat formation (Fig.2b),

where the cables are transposed and the sheaths remain in their position along the cable configuration [5, 6].

a) b)

Fig. 1: Cable laying configuration. a) Trefoil formation. b) Flat formation.

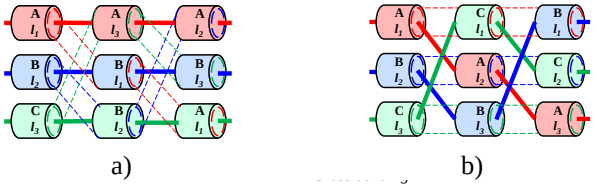

a) b)

Fig. 2. a) CB without transposition. b) CB with transposition.

In both CB configurations, the cable sheaths of each minor section are interconnected to each other through link-boxes. Fig. 3 shows the electrical scheme of a typical CB grounding system without transposition and Fig. 4 illustrates the one with transposition. Three different loops of currents (J_{l1}, J_{l2}, J_{l3}) are established by crossing the cable sheaths in each CB configuration as shown in Fig. 2, 3 and 4, while a set of three load currents J_1, J_2, J_3 passes along the three phase conductors.

Usually, coaxial cables are used to connect the sheaths of sectionalized cable joints to the link-boxes and unipolar cables to connect the sheath terminations of the minor sections to earth via grounding boxes.

For monitoring purposes, in both types of CB configurations current sensors can be located in 4 emplacements (see Fig. 3 and 4): at the beginning (origin) and ending terminals (sensors I_o and I_e) and at the first and the second crossing (sensors I_1 and I_2). The sensors at the terminals are fastened around unipolar cables while the sensors at link-boxes are fastened around coaxial cables. Consequently, in a CB configuration, the measured currents by sensors I_1 and I_2 are the difference between the currents of two different sheath loops.

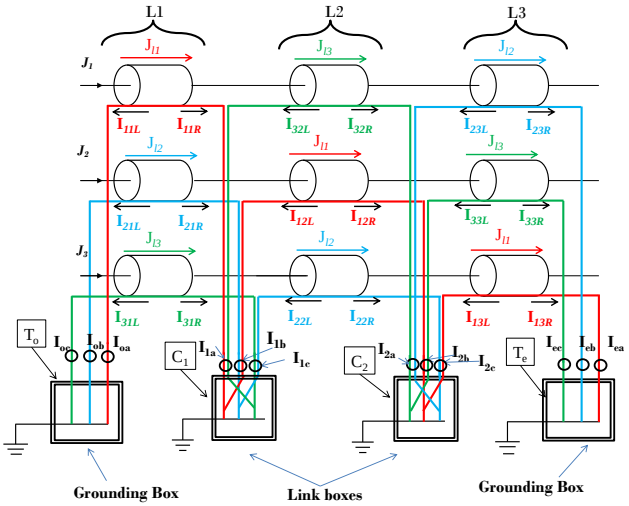

Fig. 3. CB cable system configuration without transposition.

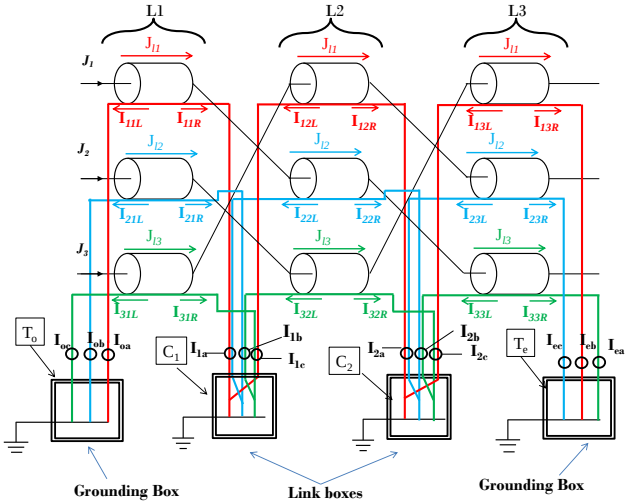

Fig. 4. CB cable system configuration with transposition.

Equation (1) shows the induced voltage in each cable sheath loop, u_{1c}, u_{2c} and u_{3c} of a CB with transposition in flat formation, due to the induced load current by the magnetic coupling between the conductors and the cable sheaths.

Where Z^{cs} is the mutual coupling impedance per unit length between a conductor and its cable sheath and Z^{cs}_{hj} is the mutual coupling impedance per unit length between the j cable sheath and a conductor located in the h laying position in a minor section in which the current is flowing. Each row of the impedance matrix [Z] multiplied by the conductor current array [J] represents the induced voltage due to the conductor currents per unit length in a minor section of the cable sheath loop [8].

Equation (2) shows the voltage induced in each cable sheath loop due to the self-impedance between the sheaths, where u_{1s}, u_{2s}, and u_{3s} represent the induced voltages in each loop due to the sheath loop currents (J_{l1}, J_{l2}, J_{l3}).

$$\left.\begin{aligned} u_{1c} &= \begin{bmatrix} L_1 & L_2 & L_3 \end{bmatrix} \begin{bmatrix} Z^{cs} & Z^{cs}_{21} & Z^{cs}_{31} \\ Z^{cs}_{21} & Z^{cs}_{31} & Z^{cs} \\ Z^{cs}_{31} & Z^{cs} & Z^{cs}_{21} \end{bmatrix} \begin{bmatrix} J_1 \\ J_2 \\ J_3 \end{bmatrix} \\ u_{2c} &= \begin{bmatrix} L_1 & L_2 & L_3 \end{bmatrix} \begin{bmatrix} Z^{cs}_{12} & Z^{cs} & Z^{cs}_{32} \\ Z^{cs} & Z^{cs}_{32} & Z^{cs}_{12} \\ Z^{cs}_{32} & Z^{cs}_{12} & Z^{cs} \end{bmatrix} \begin{bmatrix} J_1 \\ J_2 \\ J_3 \end{bmatrix} \\ u_{3c} &= \begin{bmatrix} L_1 & L_2 & L_3 \end{bmatrix} \begin{bmatrix} Z^{cs}_{13} & Z^{cs}_{23} & Z^{cs} \\ Z^{cs}_{23} & Z^{cs} & Z^{cs}_{13} \\ Z^{cs} & Z^{cs}_{13} & Z^{cs}_{23} \end{bmatrix} \begin{bmatrix} J_1 \\ J_2 \\ J_3 \end{bmatrix} \end{aligned}\right\} \quad (1)$$

$$\left.\begin{aligned} u_{1s} &= \begin{bmatrix} L_1 & L_2 & L_3 \end{bmatrix} \begin{bmatrix} Z^{ss} & Z^{ss}_{21} & Z^{ss}_{31} \\ Z^{ss} & Z^{ss}_{21} & Z^{ss}_{31} \\ Z^{ss} & Z^{ss}_{21} & Z^{ss}_{31} \end{bmatrix} \begin{bmatrix} J_{l1} \\ J_{l2} \\ J_{l3} \end{bmatrix} \\ u_{2s} &= \begin{bmatrix} L_1 & L_2 & L_3 \end{bmatrix} \begin{bmatrix} Z^{ss}_{12} & Z^{ss} & Z^{ss}_{32} \\ Z^{ss}_{12} & Z^{ss} & Z^{ss}_{32} \\ Z^{ss}_{12} & Z^{ss} & Z^{ss}_{32} \end{bmatrix} \begin{bmatrix} J_{l1} \\ J_{l2} \\ J_{l3} \end{bmatrix} \\ u_{3s} &= \begin{bmatrix} L_1 & L_2 & L_3 \end{bmatrix} \begin{bmatrix} Z^{ss}_{13} & Z^{ss}_{23} & Z^{ss} \\ Z^{ss}_{13} & Z^{ss}_{23} & Z^{ss} \\ Z^{ss}_{13} & Z^{ss}_{23} & Z^{ss} \end{bmatrix} \begin{bmatrix} J_{l1} \\ J_{l2} \\ J_{l3} \end{bmatrix} \end{aligned}\right\} \quad (2)$$

Being z^{ss} the self-sheath impedance per unit length due to the self-coupling with its own sheath and z^{ss}_{uv} the mutual coupling between the sheath loop *v*, in which the voltage is induced, and a different sheath loop located in the *u* position in a minor section in which the current is flowing. Each row of the impedance matrix [Z] multiplied by the cable sheath current array [J_l] represents the induced voltage due to the cable sheath currents in per unit length in a minor section of the cable sheath loop.

The total induced voltage in each cable sheath u_{total} (3) provokes the voltage drop in the earth resistances of both cable ends.

$$u_{total} = \begin{bmatrix} u_{1c} + u_{1s} \\ u_{2c} + u_{2s} \\ u_{3c} + u_{3s} \end{bmatrix} = -(R_1 + R_2).(J_{l1} + J_{l2} + J_{l3}).\begin{bmatrix} 1 \\ 1 \\ 1 \end{bmatrix} \quad (3)$$

Where R_1 and R_2 are the earth resistances.

Assuming that the capacitive current is negligible compared with the inductive one, by substituting (1) and (2) in (3) , the three inductive currents J_{l1}, J_{l2} and J_{l3} are determined. However, for more precision in the sheath current calculation, the capacitive component has to be considered although the resistive current associated to the insulation resistance of the cable insulation is always assumed negligible in HV cables.
The capacitive current in HV cables is expressed by (4).

$$I_C = j.\omega.c'.U \quad (4)$$

Where:

c' is the cable capacitance per unit length,
U is the operating phase voltage and
ω is the angular frequency.

The current due to the capacitive coupling depends on the total length of the CB and on the induced voltage in each minor section. The capacitive currents I_C are represented as I_{mn} where *m*=1, 2, 3 is the number of the sheath loop and *n*=1, 2, 3 the number of the section. It is assumed that the capacitive component of each minor section I_{mn} is injected in the middle of its length (i.e. $L_1/2$ for the minor section 1). This capacitive component is split into two parts I_{mnR} and I_{mnL} depending on the impedance seen from each side. For instance, in minor section 1 and sheath loop 1 the current is split as shown in (5) and (6).

$$I_{l1s1R} = \frac{Z^{ss}.\frac{L_1}{2}}{Z^{ss}.(L_1 + L_2 + L_3)} I_{11} \quad (5)$$

$$I_{l1s1L} = \frac{Z^{ss}.(\frac{L_1}{2} + L_2 + L_3)}{Z^{ss}.(L_1 + L_2 + L_3)} I_{11} \quad (6)$$

Consequently the current to be measured by each sensor placed in each phase at the beginning terminal (origin), I_o, at the first and second CB, I_1 and I_2 and at the ending terminal, I_e, of the cable system, can be expressed by (7). Similarly to the process described from (1) to (7), a set of equations can be derived to determine the current to be measured by each sensor, when CB without transposition is adopted either in flat or in trefoil formation.

$$\left.\begin{aligned}
I_{oa} &= J_{l1} - I_{11L} - I_{12L} - I_{13L} \\
I_{ob} &= J_{l2} - I_{21L} - I_{22L} - I_{23L} \\
I_{oc} &= J_{l3} - I_{31L} - I_{32L} - I_{33L} \\
I_{1a} &= (J_{l1} + I_{11R} - I_{12L} - I_{13L}) - (J_{l2} + I_{21R} - I_{22L} - I_{23L}) \\
I_{1b} &= (J_{l2} + I_{21R} - I_{22L} - I_{23L}) - (J_{l3} + I_{31R} - I_{32L} - I_{33L}) \\
I_{1c} &= (J_{l3} + I_{31R} - I_{32L} - I_{33L}) - (J_{l1} + I_{11R} - I_{12L} - I_{13L}) \\
I_{2a} &= (J_{l1} + I_{12R} + I_{11R} - I_{13L}) - (J_{l2} + I_{21R} + I_{22R} - I_{23L}) \\
I_{2b} &= (J_{l2} + I_{21R} + I_{21R} - I_{23L}) - (J_{l3} + I_{32R} + I_{31R} - I_{33L}) \\
I_{2c} &= (J_{l3} + I_{31R} + I_{32R} - I_{33L}) - (J_{l1} + I_{11R} + I_{12R} - I_{13L}) \\
I_{ea} &= J_{l1} + I_{11R} + I_{12R} + I_{13R} \\
I_{eb} &= J_{l2} + I_{21R} + I_{22R} + I_{23R} \\
I_{ec} &= J_{l3} + I_{31R} + I_{32R} + I_{33R}
\end{aligned}\right\} \quad (7)$$

B. Study Cases/ Cable modeling

A 220kV CB cable system with the parameters stated in Table I, was modeled using the ATP software. Furthermore, a model based on the analytical equations, stated in the previous subsection, was applied using the mathematical software Matlab. The cable was modeled in flat formation in a CB configuration with and without transposition and in trefoil formation without transposition.

A comparison between ATP and Matlab models is performed to check both of them. As it is shown in Tables II.a and II.b, a good agreement between the results obtained applying the analytical equations and those calculated with ATP is achieved, which guarantees the implementation correctness of the ATP model. As with the ATP model a more accurate simulation can be achieved, this model is considered as reference in this research.

TABLE I
Cable Parameters

Parameters	**Value**
Raduis of the conductor (mm)	27.6
Raduis of insulation (mm)	51.9
Relative permativity of insulation	2.5
Exterior sheath diameter (mm)	114.5
Interior sheath diameter (mm)	109.68
Sheath resistivity (Ω·m)	$7.2034.10^{-8}$
Conductor resistivity	$2.2952.10^{-8}$
Ground resistance Ω	0.2
Separation between phases (cm)	42.5
L_1(m)	540
L_2(m)	600
L_3(m)	660
Load current for the simulations (A)	1200
Power factor	1

TABLE II.a.
Comparison between ATP and Matlab Results from the Sensors at The Terminals under Normal Conditions

Sensors		**I_{oa} (A)**	**I_{ob} (A)**	**I_{oc} (A)**	**I_{ea} (A)**	**I_{eb} (A)**	**I_{ec} (A)**
Flat formation in CB without transposition	ATP	70.0	47.6	60.9	46.5	60.2	70.0
	Matlab	68.0	50.5	59.3	50.5	59.3	68.0
Flat formation in CB with transposition	ATP	55.3	54.9	64.0	55.0	54.3	64.2
	Matlab	54.8	54.3	64.7	54.4	53.7	63.5
Trefoil formation	ATP	53.1	53.1	52.5	52.5	52.5	52.5
	Matlab	53.0	53.0	53.0	52.4	52.4	52.4

TABLE II.b
Comparison between ATP and Matlab Results from the Sensors at the Crossing under Normal Conditions

Sensors		I_{1a} (A)	I_{1b} (A)	I_{1c} (A)	I_{2a} (A)	I_{2b} (A)	I_{2c} (A)
Flat formation in CB without transposition	ATP	114	78.4	78.5	87.3	123	121
	Matlab	114	79.0	79.0	87.6	122	121
Flat formation in CB with transposition	ATP	115	114	97.3	105	106	89.0
	Matlab	115	114	98.0	105	106	89.4
Trefoil formation	ATP	93.0	93.0	93.0	101	101	101
	Matlab	93.3	93.3	93.3	101	101	101

The results also indicate that the sheath currents in CB configuration with transposition of flat formation are smaller than those without transposition. Therefore, it can be corroborated in this paper that cable transposition should be used for CB in flat formation, while it is not required for CB in trefoil formation, in which the smallest sheath currents are achieved.

C. Defect detection criterion by the total induced current in the cable sheath

A general criterion for detecting defects in cable sheath was introduced in [8] on the basis of the total induced current in the cable sheath (TICS). The TICS in each sensor is expressed in per-unit being referred to its expected value in the normal operation condition (no defect). The resulted values are classified into 4 discrete levels #0, #1, #2, #3 and #4 (see Table III), each level represents a change in the sheath current (I_s) in case of defect with respect to the expected current for normal operation (no defect).

Level #1 is used to represent the current level in normal conditions (no defect) with a tolerance of 25%, taking into account the influence parameters such as: percentage of unbalance in the minor sections, load current, cable characteristics, measuring uncertainties, temperature effect etc. The transition limit between level #2 and #3 (7.5pu) and between #3 and #4 (12.5pu) are chosen with an order of magnitude greater (10 times) than the threshold to pass from #0 to #1 and from #1 to #2.

A Simple operation code (SOC) is obtained to identify different types of defects that might occur in the cable sheath through 12 digits. The first set of three digits represents the currents measured by the sensors located at the beginning terminal T_o (I_{oa}, I_{ob}, I_{oc}), the second set of three digits corresponds to the currents at the ending terminal T_e (I_{ea}, I_{eb}, I_{ec}). The third set corresponds to the currents at the first linkbox C_1 (I_{1a}, I_{1b}, I_{1c}) and the last set to the currents at the second linkbox C_2 (I_{2a}, I_{2b}, I_{2c}). The SOC is split in two sub-SOCs, terminal code C_o,C_e and cross code C_1, C_2

TABLE III
Criterion of Defect Classification

Condition	Classification	Level
$Is \leq 0.75pu$	Below the normal expected value	#0
$0.75pu < I_s \leq 1.25pu$	Normal expected value	#1
$1.25pu < I_s \leq 7.5pu$	Above the normal expected level	#2
$7.5pu < I_s \leq 12.5pu$	Very above the normal expected level	#3
$12.5pu < I_s$	Ultra above the normal expected level	#4

For low load currents the percentage of the inductive current in the total current decreases, while the percentage of the capacitive current increases. This effect leads to the instability of the diagnostic codes, obtained from TISC, under low levels of load current. In order to mitigate this effect a complementary method on the basis of subtracting the current induced due to capacitive coupling is proposed.

D. Improved defect detection criterion

The capacitive current subtraction (CCS) method proposed allows obtaining only the inductive current (J_{l1}, J_{l2} and J_{l3}) in each cable sheath loop by subtracting the capacitive current. The capacitive current component is obtained by ATP considering a zero load current. Alternatively the inductive current can be also determined by assuming a negligible relative permittivity. Both procedures permit to verify if the inductive current is correctly determined when the CSS method is applied. Fig.5a shows the almost direct proportionality between the total circulating current in the sheath and the inductive current for a high percentage of load current, where the capacitive component is too small and does not depend on the load current. Fig. 5b shows the phase displacement of the total induced current in the cable sheath, which is nearly equal to the inductive current for high load currents, while it is close to the capacitive current for low levels of load current.

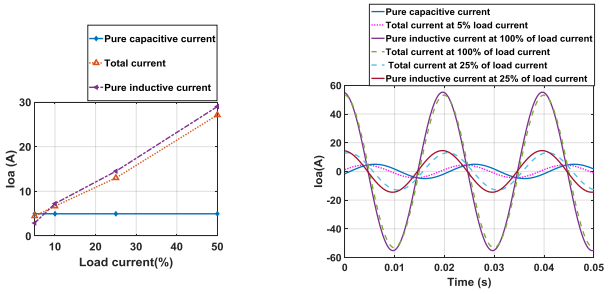

(a) (b)

Fig. 5: a) Relation between sheath currents and load currents b) Influence of high and low load current levels on sheath currents.

The SOC that will be obtained after applying the CCS method, are based on the calculations of the per unit values of the total induced current detected by a sensor, under a certain defect (I_d) subtracted from the capacitive current detected by the same sensor under the same defect (I_{dc}). This value is divided by the expected value of the total induced current under normal condition at a certain load level (I_N), subtracted from the capacitive current under normal condition (I_{Nc}), as shown in (8). It is important to note that this method requires phasor sheath current measurements.

$$I_{p.u} = \frac{I_d - I_{dc}}{I_N - I_{Nc}} \tag{8}$$

Where,

I_d is the sheath current in case of a defect,
I_{dc} is the capacitive component of I_d,
I_N is the sheath current in normal condition (no defect) and
I_{Nc} is the capacitive component for the I_N.

III. TYPES OF DEFECTS

This section is dedicated to show different types of defect that may occur in the cable sheaths and how these defects affect the diagnostic codes $C_o C_e$ and $C_1 C_2$. The criterion presented in section II is used for the analysis. The evaluation is initially performed assuming that the load current is 100% (1200 A for the studied case) which is not usually reached in the normal operation of a real cable.

The influence of reducing the load current on the diagnostic codes, obtained from TICS $C_o C_e$ and $C_1 C_2$ is also studied in this section. The values of the diagnostic codes are also shown after applying the CCS method.

A. *Open circuit fault in sheath loop*

This type of defect occurs when a sheath is disconnected to ground. It is assumed that the defect might present at different positions along each loop (T_o, C_1, C_2 and T_e) see Fig. 3 and 4. Table IV shows the codes obtained from the sensors located at the terminals ($C_o C_e$) and at the linkboxes ($C_1 C_2$) in case of occurrence of open circuit defect at different loops. It is important to note that same SOC is obtained independently on the location of the open circuit along the same sheath loop.

By applying the TICS method, presented in subsection II.C, on this defect, a good the stability is maintained up to the 25% of the applied load current (see Table IV). A significant instability of the codes appears for lower load currents even when the open circuit occurs along the same loop. Table V shows the instability of the codes at 17% and 5% of load current when the disconnection occurs at different positions along loop1.

TABLE IV
SOC under Open Circuit Fault in Sheath Loop

Location	Formation	Load current (%)	$C_o C_e$/ $C_1 C_2$ TICS
Loop1	Trefoil	100-25	011,110/001,100
	Flat	100-25	011,011/100,100
Loop 2	Trefoil	100-25	101,011/100,010
	Flat	100-25	101,101/010,010
Loop 3	Trefoil	100-25	110,101/010,001
	Flat	100-25	110,110/001,001

TABLE V
Influence of Low Percentage of Load Current on the SOCs

Cable formation	defect along loop1	I_{Load} (%)	$C_o C_e / C_1 C_2$ TICS	$C_o C_e / C_1 C_2$ CCS
Trefoil	T_o	17	011,010/011,100	011,110/001,100
		5	011,110/221,101	
	L_1	17	001,011/001,100	
		5	111,111/001,111	
	L_2	17	001,011/011,100	
		5	111,111/221,100	
	T_e	17	011,010/011,101	
		5	011,110/221,101	
Flat	T_o	17	011,011/100,011	011,011/100,100
		5	011,011/122,110	
	L_1	17	001,001/100,010	
		5	101,101/100,111	
	L_2	17	001,001/100,011	
		5	111,111/122,010	
	T_e	17	011,011/101,010	
		5	011,011/122,110	

However, by applying the CCS method, the stability is maintained for load currents from 5% to 100% (see the last two columns in Table V). It is important to note that if the open circuit occurs at the cable terminals independently on the load current applied, the sheath current measured by the sensors placed in those positions will be zero, which permits the localization of this defect at once.

From Tables IV and V, it is noticed that by applying the improved CCS method the defect can be detected and localized either at the terminal or at the linkboxes for load current greater than 5%.

B. *Breakdown between two sectionalized sheaths*

When the insulation of the coaxial cables used to connect the sheaths to each other fails or when the insulation between sectionalized sheaths of the joint fails, a short circuit between two sheaths occurs.

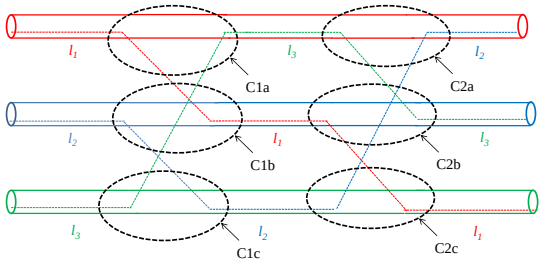

Fig. 6: Geometrical sectionalized sheaths in CB configuration without transposition (trefoil formation).

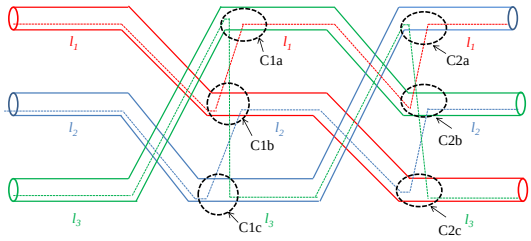

Fig. 7: Geometrical sectionalized sheaths in CB configuration with transposition (flat formation).

This fact leads to an increase in the current to be measured by the sensors and forms the codes presented in Tables VI and VII. This kind of defect has been implemented with the ATP software by interconnecting a very small resistance between the metal sheaths coming from a certain cable joint. Fig. 6 shows the geometrical sectionalization of sheaths in a CB configuration without transposition.

Although the cable sheaths in a cable joint of a CB configuration with transposition maintain their continuity (electrical position), they are physically sectionalized as shown in Fig.4 and 7. This is done in order to return the cable sheaths to their original position. A breakdown between two sectionalized sheaths is critical in a CB with and without transposition as well. Tables VI and VII show the SOCs obtained from the current detected in each sensor for different percentages of load current in trefoil formation (CB without transposition) and in flat formation (CB with transposition) respectively. By analyzing the results shown, it can be noticed that the codes $C_o C_e$ and $C_1 C_2$ are changeable according to the position where the defect occurs, which permits detecting and localizing the defect easily either in flat or trefoil

formation. After applying the CCS method, the codes maintain the stability at low levels of load current. Consequently, the CCS method is more efficient than the simple operation code method.

TABLE VI
SOC under Breakdown between Sheaths in Trefoil Formation
(CB without Transposition)

Location of defect	load current (%)	$C_o,C_e/C_1,C_2$ TICS	$C_o,C_e/C_1,C_2$ CCS
C_{1a}	100-25	414,133/223,232	414,133/223,232
	17	414,122/223,222	
	5	313,122/324,222	
C_{1b}	100-25	441,313/322,222	441,313/322,222
	17	441,212/322,222	
	5	331,212/432,222	
C_{1c}	100-25	144,331/232,322	144,331/232,322
	17	144,221/232,222;	
	5	133,221/243,222	
C_{2a}	100-25	133,441/223,232	133,441/223,232
	17	122,441/223,222	
	5	122,331/324,222	
C_{2b}	100-25	313,144/322,222	313,144/322,222
	17	212,144/322,222	
	5	212,133/432,222	
C_{2c}	100-25	331,414/232,322	331,414/232,322
	17	221,314/232,222	
	5	221,313/243,222	

TABLE VII
SOC under Breakdown between Sheaths in Flat Formation
(CB with Transposition)

Location of defect	Load current (%)	$C_o,C_e/C_1,C_2$ TICS	$C_o,C_e/C_1,C_2$ CCS
C_{1a}	100-25	414,313/243,232	414,313/243,232
	17	414,312/243,232	
	5	313,212/232,243	
C_{1b}	100-25	144,132/433,322	144,132/433,322
	17	144,132/322,322	
	5	133,122/222,333	
C_{1c}	100-25	441,331/324,223	441,331/324,223
	17	441,331/224,223	
	5	331,221/223,234	
C_{2a}	100-25	313,414/232,232	313,414/232,232
	17	313,413/222,232	
	5	212,312/222,243	
C_{2b}	100-25	132,144/322,322	132,144/223,322
	17	132,133/222,322	
	5	122,122/212,433	
C_{2c}	100-25	331,441/223,223	331,441/223,223
	17	331,441/222,223	
	5	221,231/122,234	

C. *Defect of installation in linkbox*

This section is focused on showing different scenarios of wrong sheath connections in linkboxes and their effect on the sheath currents. As in this paper the flat and trefoil formations have different CB configurations (with and without transposition), several scenarios can occur in each one of them. Fig. 8 shows the erroneous sheath connection scenarios that were studied for trefoil formation (see Fig.2a), while Fig. 9 shows those studied for flat formation (see Fig.2b). Table VIII shows the codes obtained from both configurations for different percentages of load current, before and after applying CCS method.

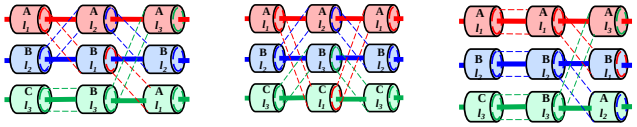

a) b) c)

Fig. 8: Wrong sheath connection scenarios in trefoil formation
a) scenario 1 b) scenario 2 c) scenario3.

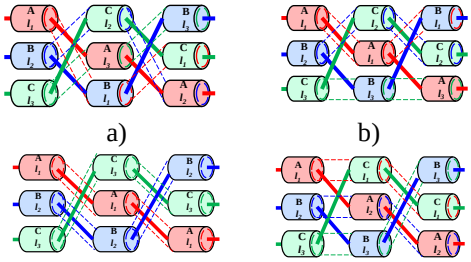

a) b) c) d)

Fig. 9: Wrong sheath connection scenarios in flat formation
a) scenario 4 b) scenario 5 c) scenario 6 d) scenario7.

TABLE VIII
SOC under Wrong Connection in Linkbox

Defect scenario	Load current (%)	$C_o,C_e/C_1,C_2$ TICS	$C_o,C_e/C_1,C_2$ CCS
Scenario 1	100-25	133,331/220,433	133,331/220,433
	17	143,331/220,422	
	5	122,221/330,222	
Scenario 2	100-25	333,333/333,444	333,333/333,444
	17	343,333/333,333	
	5	222,222/444,222	
Scenario 3	100-25	333,333/000,444	333,333/000,444
	17	333,333/000,333	
	5	222,222/000,222	
Scenario 4	100-5	222,222/222,222	222,222/222,222
Scenario 5	100-25	332,332/223,224	332,332/223,224
	17	332,332/223,234	
	5	221,221/222,234	
Scenario 6	100-17	444,444/444,444	444,444/444,444
	5	333,333/333,444	
Scenario 7	100-25	333,333/333,333	333,333/333,333
	17	333,333/322,433	
	5	222,222/222,444	

Due to the high values obtained in the sheath currents caused by these defects, the codes obtained from TICS maintain the stability up to 17% of the load current at some scenarios e.g. scenario 4 and 6. Whereas after applying the CCS method, the codes maintain the stability for a wide range of load current up to 5% for all the studied scenarios.

D. *Flooding in link box defect*

Flooding in linkboxes causes a 3 phased short circuit in linkboxes which leads to an excess in the sheath currents measured. The obtained codes form this defect at different locations along the CB system in trefoil and flat formation are shown in Tables IX and X. It can be observed that this defect provokes the highest increase in the load currents. As a result of that, it is observed that C_o in trefoil formation and C_o, C_e in

flat formation maintain stability till 17% of load current. Nevertheless, to guarantee the stability of the SOC obtained from all the measuring points, CCS method has to be applied.

TABLE IX
SOC under Flooding in Linkboxes in Trefoil Formation

Defect location	Load current (%)	$C_o,C_e/C_1,C_2$ TICS	$C_o,C_e/C_1,C_2$ CCS
LB1	100-25	444,333/333,333	444,333/333,333
	17	444,222/333,222	
	5	333,222/444,222	
LB2	100-25	333,444/333,333	333,444/333,333
	17	333,444/333,222	
	5	222,444/444,222	
LB1&LB 2	100-25	444,444/000,000	444,444/000,000
	17	444,333/000,000	
	5	333,333/111,000	

TABLE X
SOC under Flooding in Linkboxes in Flat Formation

Defect location	Load current (%)	$C_o,C_e/C_1,C_2$ TICS	$C_o,C_e/C_1,C_2$ CCS
LB1	100-25	444,333/444,333	444,333/444,333
	17	444,333/343,333	
	5	333,222/232,444	
LB2	100-25	333,444/333,333	333,444/333,333
	17	333,444/222,444	
	5	444,444/343,444	
LB1&LB 2	100-25	444,444/444,444	444,444/444,444
	17	444,444/343,444	
	5	333,333/232,444	

IV. UNBALANCE IN MINOR SECTIONS INFLUENCE

This section is devoted to show the influence of the percentage of unbalance in the minor sections of a CB cable system under 100% of load current. The study in this section is started by taking the length of the middle section as the reference length. Whilst the lengths of the other two sections are considered as a percentage of the reference length (the length of the middle section), assuming ± 30% is the highest percentage of unbalance that might occur in a CB cable system. As the percentage of unbalance increases, the circulating current in the cable sheath increases. This might affect the SOC obtained. Fig.10 illustrates the code obtained at almost all the possible combinations of unbalance that might occur in a CB cable system, in case of inadequate sheath connection in linkbox scenario 4.

From Fig. 10, it is observed that the code shown in Table VIII, maintained the stability at almost 53% of the possible combinations of unbalance (highlighted by green). 20% of them are stable at only one sub-SOC either C_o,C_e or C_1,C_2(highlighted by blue). However different codes are obtained at 28% of the possible combinations of unbalance (Highlighted by yellow and pink).

It is important to note that the yellow highlighted zones in Fig.10, representing 24.4% of the possible combinations, are likely to have the same tendency of the change in the sheath current e.g. the code obtained at L1/L2=0.7 and L2/L3=1.3 is 022,202, 202,022 which means that at all measurement position, the current increases in two phases and decrease in the third one which is the same tendency of the code produced at L1/L2=1.3 and L2/L3=0.7.

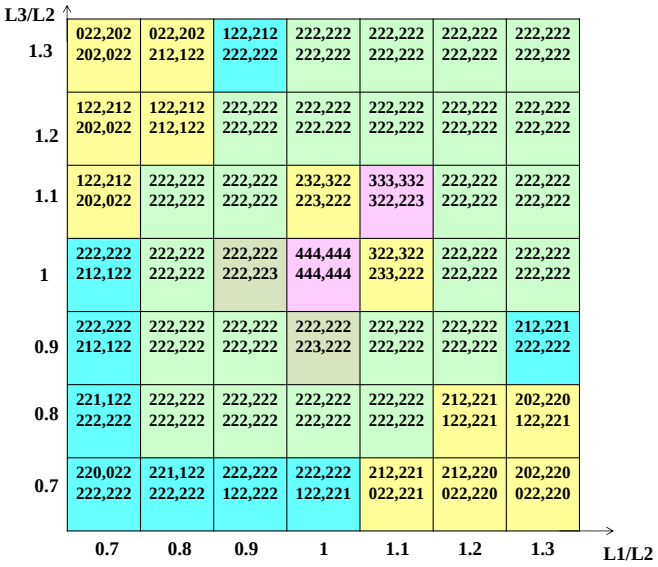

Fig.10 : influence of the percentage of unbalance on the SOCs.

V. GENERALIZATION

It has been shown that in case of open circuit fault in the sheath loop, the sheath current decrease contrary to the rest of the cases where the sheath currents increase. Consequently, the codes obtained in case of open circuit in sheath loop are between #0 and# 1. However, in case of occurrence of any of the other types of defects, the sheath current increases which leads to codes #2, #3 and #4. In all the defects studied in this paper, the code digits are changeable according to the location of the defect.

Consequently the flow chart illustrated in Fig. 11 is defined to detect and localize cable sheath defects. This flow chart starts by measuring the sheath current with all the sensors (I_{ok}, I_{1k}, I_{2k} and I_{ek}) where k=a, b and c. If one of the sensors at the terminal I_{ok} or I_{ek} measures approximately zero, then the identification and localization of the open circuit fault is possible, considering the position of the sensor that measures approximately zero. Otherwise, the TICS method can be applied as long as the load current is greater than 25%. If the obtained codes are composed of zeros and ones, then the defect is identified to be open circuit fault at the joints. On the other hand, if the obtained code is a standard code as those presented in section III, the defect can be identified.

However it is important to note that the in flat formation, the produced code from flooding defect in both linkboxes (see Table X) and one produced from the inadequate connection in linkboxes scenario 6 (see Table VIII) are the same. Thus in this particular case, one can distinguish between both defects by just checking the linkboxes visually. For low levels of load current is recommended to apply the CCS method. Otherwise the SOCs have to be recalculated according to the unbalance in the minor sections in the particular studied case.

To guarantee a perfect detection and localization at least measurement at two different locations is required (I_o, I_1, I_2 and I_e sites). However, at some cases, the localization and the identification of the defect can be performed by just measuring at only one location. For example: in case of breakdown between sheaths at C_{1a} in trefoil formation (Table VI), by just

obtaining the measurements at I_o (C_o, 414), the defect can be identified and localized due to the unrepeatability of the code in the other studied defects (see Tables IV - X).

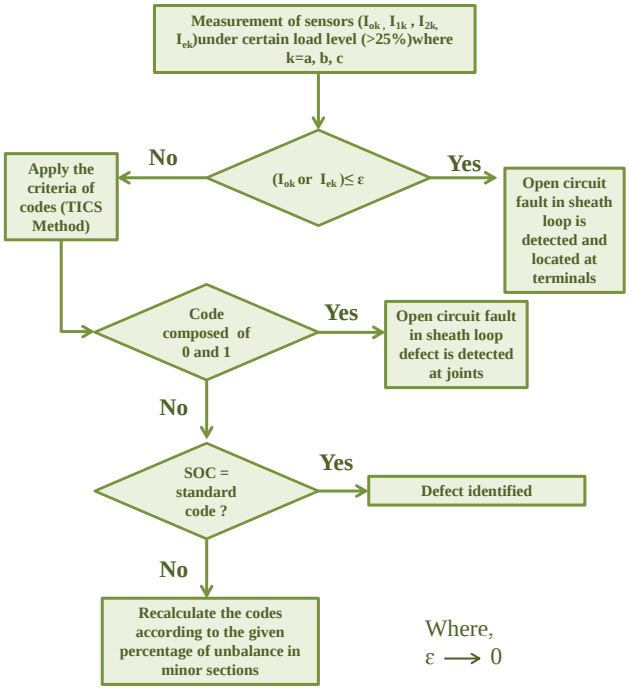

Fig. 11: Flow chart of the detection criteria.

VI. Real Measurements Validation

A real case study is presented in this section, for a 220 kV cable system and its parameters stated in Table XI, considering the lengths of the minor sections are: L1=288m, L2=340m and L3=260m, i.e. L1/L2=0.84 and L3/L2=0.76.The cable belongs to the Spanish TSO and it is installed in CB with transposition configuration in flat formation and its sheath currents have been monitored [9]. The measurements were taken only from an ending terminal of a cross bonding configuration (I_e) over 20 days under a maximum load current of approximately 500 A, which is almost 50% of the rated load current that can be applied. All the measurements have been normalized to 500 A of load current. The mean and the standard deviation of the measured data were considered for analysis.

An unexpected increase in the sheath currents was detected. Furthermore, a significant unbalance between different cable sheath currents was observed in the measuring point I_e. The developed criterion of SOC was applied, by means of calculating the per-unit values of the sheath current (in case of defect), obtained via measurements with the base value of the expected sheath current (under normal condition) obtained via simulations as shown in Table XII. Considering the percentage of unbalance between lengths in minor sections, it was found that the code obtained, corresponds to the inadequate sheath connection scenario 4 illustrated in Fig. 9a and 10.

This defect has been simulated by means of ATP software. Also a Matlab code has been implemented using the analytical equations under this defected scenario, in order to compare the results obtained from the measurements with those obtained from the simulations and from the calculations, Table XIII shows a good agreement between the measured, simulated and calculated results.

TABLE XI
Parameters of the Measured Cable

Parameters	Value
Raduis of the conductor (mm)	21
Raduis of insulation (mm)	37
Exterior sheath diameter (mm)	84
Sheath resistivity(Ω·m)	$2.2.10^{-7}$
Sepation distance (cm)	30

TABLE XII
Per-Unit Values Based on the Measurement Results

Measured sensors	I_{ea}	I_{eb}	I_{ec}
Per unit values	1.9	2.7	2.47
Code	2	2	2

TABLE XIII
Comparison between measured, simulated and calculated results

Sensor	I_{ea} (A)	I_{eb} (A)	I_{ec} (A)
Mean of the measured data ± Standard deviation	34.7±3.4	65.3±5.1	59.8±3.5
ATP simulated results	35.6	65.8	54.4
Matlab calculated results	34	67.5	58.2

CONCLUSION

This paper proposes a new method for the detection and localization of 4 types of defects that might occur in the cable sheath of a cross bonding configuration. Criterion of codes from #0 to #4 is developed in order to represent the level of change of the sheath current in case of defect. This criterion can be applied at load current of 25% or greater. At low levels of load current (< 25%), a complementary method has been presented to remove the capacitive current from the total induced current in the sheath in order to maintain the stability.

The criterion proposed in this paper can be also applied on different percentages of unbalance in the minor sections that might exist in CB cable grounding system.

References

[1]X. Dong, Y. Yang, C. Zhou and D. Hepburn, "Online Monitoring and Diagnosis of HV Cable Faults by Sheath System Currents", *IEEE Transactions on Power Delivery*, vol. 32, no. 5, pp. 2281-2290, 2017.

[2]Mingzhen Li, W. Zhou, Chunlin Wang, Leiming Yao, Mengting Su, Xiaojun Huang and C. Zhou, "A novel fault localization method based on monitoring of sheath current in a cross-bonded HV cable system", *2017 IEEE Electrical Insulation Conference (EIC)*, 2017.

[3]Y. Yang, D. Hepburn, C. Zhou, W. Zhou and Y. Bao, "On-line monitoring of relative dielectric losses in cross-bonded cables using sheath currents", *IEEE Transactions on Dielectrics and Electrical Insulation*, vol. 24, no. 5, pp. 2677-2685, 2017.

[4]M. Marzinotto and G. Mazzanti, "The Feasibility of Cable Sheath Fault Detection by Monitoring Sheath-to-Ground Currents at the Ends of Cross-Bonding Sections", *IEEE Transactions on Industry Applications*, vol. 51, no. 6, pp. 5376-5384, 2015.

[5]515-2011 IEEE Standard for the Testing, Design, Installation, and Maintenance of Electrical Resistance Trace Heating for Industrial Applications - Redline. (2011).

[6]575-2014 IEEE Guide for Bonding Shields and Sheaths of Single-conductor Power Cables Rated 5 Kv through 500 Kv. (2014).

[7]P. Simón Comín and F. Garnacho, *Cálculo y diseño de líneas eléctricas de alta tensión*. Madrid: Ibergarceta, 2011.

[8] A. Khamlichi, M. Adel, F. Garnacho and J. Rovira, "Measuring cable sheath currents to detect defects in cable sheath connections", *52nd International Universities Power Engineering Conference* (UPEC), 2017.

[9] A. Burgos, G. Donoso, B. García, "Sheath currents monitoring in high voltage isolated cables", *International Council on Large Electrical Systems* (CIGRE), 2016.